processes

MDPI

Article

Design and Analysis of Comprehensive Solar Utilization System Based on Photovoltaic Concentration and Spectral Splitting

Zhipeng He and Yizhi Tian *

College of Electrical Engineering, Xinjiang University, Urumqi 830017, China
* Correspondence: torsionscale@163.com

Abstract: In order to address the issue of a solar utilization system with low efficiency, this paper designs a new solar conversion system based on photovoltaic concentration and spectral splitting. The system concentrates sunlight through a Fresnel lens and uses a hollow concave cavity to evenly distribute the incident energy flow. The spectral splitting medium separates the useful irradiance for the PV cell from those wavelengths that are more suited to heat generation. By considering the available wavelength of photovoltaic cells, the GaAs cell and a ZnO nanofluid were selected for this paper. It was found that installing the hollow concave cavity improved the spot uniformity of the PV cell surface by 17%. The output efficiency of the system under various circumstances was analyzed. The results show that at a concentration ratio of 50 and a light intensity of 1000 W/m^2, photoelectric conversion efficiency increased by 0.81%. When compared to direct concentration, the photoelectric conversion efficiency increased by at least 7%. Meanwhile, the comprehensive electrical efficiency was 36.7%, which is higher than that of the normal concentration PV and comprehensive thermal system.

Keywords: comprehensive utilization of solar energy; Fresnel lens concentration; spectral splitting; ZnO nanofluid; GaAs cell; photoelectric conversion; photothermal conversion

Citation: He, Z.; Tian, Y. Design and Analysis of Comprehensive Solar Utilization System Based on Photovoltaic Concentration and Spectral Splitting. *Processes* **2023**, *11*, 1944. https://doi.org/10.3390/pr11071944

Academic Editor: Sara Pescetelli

Received: 5 June 2023
Revised: 24 June 2023
Accepted: 26 June 2023
Published: 27 June 2023

1. Introduction

In the traditional photovoltaic power generation system, the photovoltaic cells are subject to the characteristics of the material; only 15~20% of the solar radiation is converted into electric [1]. By increasing the energy flow density per unit area, the efficiency of PV cells can be improved, and the cost of PV cells can be reduced [2]. The absorption of solar radiation by photovoltaics during operation will increase the temperature of the cell. Adding a heat collection module to the back of the PV cell to collect the waste heat for reuse is helpful for improving the comprehensive utilization rate of solar energy [3]. Xiaolong WU [4] designed a V-shaped trough, low-power concentrating photovoltaic/thermal system (CPV/T). By symmetrically installing two flat mirrors on both sides of the PV panel, sunlight was concentrated onto the PV panel and formed a high energy density spot. The system was tested and improved the power generation efficiency by 19.9% on average when compared to the nonconcentrating system. Being limited by the number of plane mirrors installed, the system can only achieve low power focusing, and the concentrating ratio is 5~10 times [5]. In the process of concentration, the surface of PV cells will have an uneven energy flow density, which will cause thermal spot effects and reduce the efficiency of PV cells [6]. Zhuling Jin [7] proposed the combination of Fresnel point-focus spotlighting with a PV/T system. The average power of the system is 27.36%, and the instantaneous maximum thermal efficiency is 30.02%. However, when the concentration ratio is greater than 15 times, the temperature of the PV cell also increases significantly, causing a decrease in the photovoltaic conversion efficiency of the PV cell [8].

In order to ensure that the PV cells work at an appropriate temperature while obtaining high-quality thermal energy, some scholars proposed the use of spectral-splitting technology in solar utilization systems [9]. The principle of solar spectrum splitting is to separate out the sunlight in the spectral band that is less than the band gap energy of the PV cells. This idea reduces the ineffective radiance to the PV cells from the energy acquisition path, thus increasing system conversion efficiency [10]. The main common spectral splitters mainly include a solid-film spectral splitter and a liquid spectral splitter. Solid-film spectral splitters use the mutual interference of different materials on the solar spectrum to give the filter good transmissibility or reflectivity over a specific wavelength range [11]. Crisstomo [12] designed a multilayer film spectral splitter made of SiN_x/SiO_2. This splitter reflects sunlight in specific wavelengths to the silicon PV cells and transmits light in the remaining wavelengths to the thermal receiver. The experiment showed that the efficiency of the cell after spectral splitting increased by 9.2% compared to that without spectral splitting. However, there are problems in complex splitting structures and high fabrication costs in designing solid-film spectral splitters [13]. Unlike the solid-film splitter, the liquid splitter is used to separate the solar spectrum, and it can also be used as a heat transfer medium to reduce the heat transfer loss of the system [14]. The common liquid spectral splitting media include silicone oil, propylene glycol, a $CoSO_4$ solution, and nanofluids [15–18]. Ju [19] investigated the effects of the material, splitting particle concentration, and the splitting window of a nanofluid on the performance of the splitter. The feasibility of a nanofluid as a spectral-splitting medium in a practical system was demonstrated.

At present, the research on the design of comprehensive solar energy utilization systems is mostly aimed at CPV/T systems. Although low-grade heat energy can be obtained, the problem of heating up the cell has not been fundamentally solved. Therefore, we designed a comprehensive solar energy utilization system based on a Fresnel lens concentrator and liquid spectral-splitting technology. The system uses a hollow concave cavity to evenly distribute the flow of incident light. This paper establishes the geometric model of a Fresnel lens and a hollow concave cavity, using the ray-tracing method through TracePro to analyze the performance of the concentrator. At the same time, according to the process of system energy transfer conservation, efficiency models of photoelectric and photothermal conversion were established, and the effect of different design parameters on the system characteristics was analyzed.

2. System Design Based on Ray-Tracing Method

The structure of the system is shown in Figure 1, which is composed of a Fresnel lens, a hollow concave cavity, a spectral-splitting splitter, and a PV cell. Depending on the wavelength and content of the solar spectrum, lines of three colors are used to indicate the different wavelengths of light. For example, green for visible light, red for infrared light, and purple for ultraviolet light. When the system is in operation, the high-energy-density light is concentrated by the Fresnel lens. The hollow concave cavity is filled with a liquid spectral-splitting medium. The visible wavelengths are transmitted through the medium to the cell for photoelectric conversion, while the infrared wavelengths are absorbed by the spectral-splitting medium.

The temperature of the liquid spectral-splitting medium increases after absorbing solar radiation energy. Then, the medium inflows the heat exchanger and transfers heat using water to obtain high-temperature water vapor, which is converted into electric energy through the power generation system. The structure of the spectrum splitting and photovoltaic/thermo hybrid concentration solar system are shown in Figure 2.

The system splits the solar spectrum energy via the concentrating and spectrum-splitting subsystem. The Fresnel lens concentrator, a hollow concave cavity splitter, which concentrates the PV cell and spectrum splitting medium, was designed according to the sunlight energy variation characteristics of the concentrator and spectrum splitter.

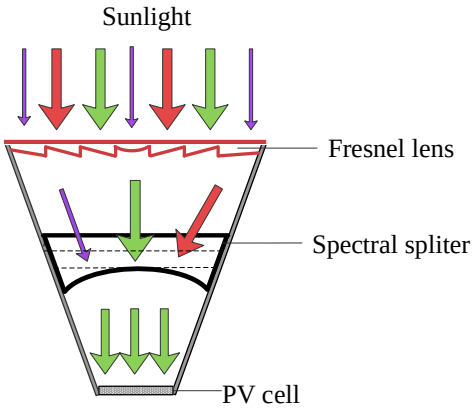

Figure 1. Structure of concentrating and spectral-splitting subsystem.

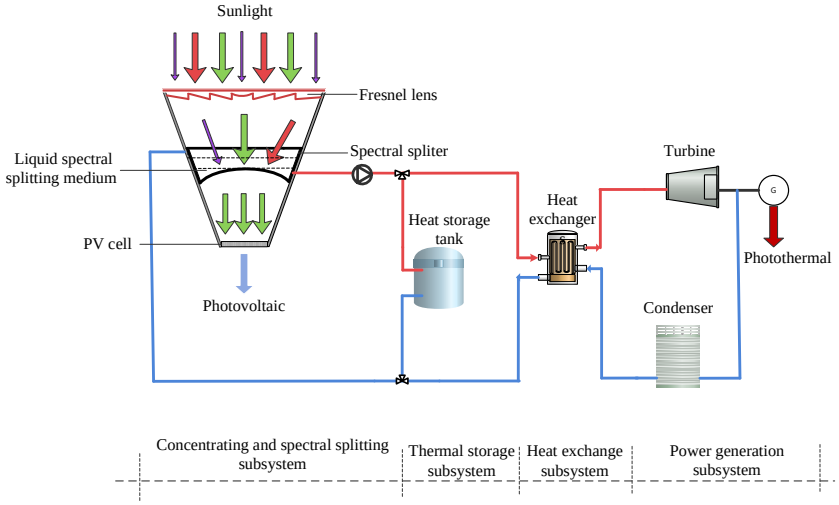

Figure 2. Structure of spectrum splitting and photovoltaic/thermo hybrid concentration solar system.

2.1. Design of Fresnel Lens Concentrator

The Fresnel lens is composed of a series of concentric arris that is used to concentrate the light incident on the lens surface to a common focus. The inclination angle of each ring band determines the focusing position. In this paper, the inclination angle of each ring bevel of the Fresnel lens is discussed. The schematic diagram of the Fresnel lens is shown in Figure 3. The light enters from point A on the upper side of the Fresnel lens and then exits from point B after refraction and intersects the optical axis on the other side of the lens F′; f is the object distance, and f′ is the image distance. The distance from point A to the axis of the lens is r. The distance from point B to the plane of the lens is h. The distance from B to the axis of the lens is r′. The tooth pitch of the lens is b.

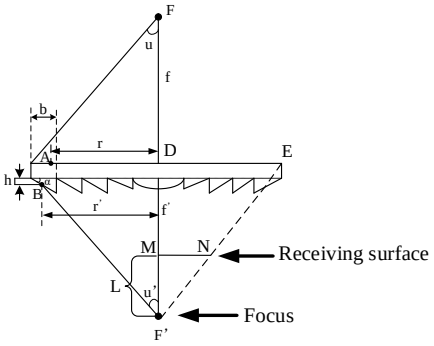

Figure 3. The schematic diagram of the Fresnel lens.

From the geometric relationship, we know that

$$h = \frac{b}{2} \tan \alpha \tag{1}$$

$$\sin u = \frac{r}{\sqrt{r^2 + f^2}} \tag{2}$$

$$\sin\ u' = \frac{r'}{\sqrt{r'^2 + (f' - h)^2}} \tag{3}$$

According to the law of light propagation, when a single light is incident on a small inclined plane, the formula for the inclination angle of the plane can be obtained:

$$\tan \alpha = \frac{\sin u + \sin\ u'}{\sqrt{n^2 - \sin^2 u} - \cos\ u'} \tag{4}$$

where n is the refractive index of the Fresnel lens. In the solar concentrator design, it is generally considered that the sunlight is incident vertically on the concentrator from infinity [20]. Therefore, $f \to \infty$, $u = 0°$; therefore, Equation (4) can be simplified as

$$\tan \alpha = \frac{\sin\ u'}{n - \cos\ u'} \tag{5}$$

Substituting Equation (3) into Equation (5) gives

$$\tan \alpha = \frac{r'}{n\sqrt{r'^2 + (f' - h)^2} - f' + h} \tag{6}$$

The center height of the inclined plane h is far less than the focal length f, so the formula of the slope angle can be derived:

$$\tan \alpha = \frac{r'}{n\sqrt{r'^2 + f'^2} - f'} \tag{7}$$

Concentration ratio is the main parameter that characterizes the light gathering performance of a Fresnel lens [20]. The concentration ratio is defined as the ratio of the input surface to the output surface. The geometric relationship between the Fresnel lens and the receiving surface is shown in Figure 3. In the Fresnel concentrator, as the receiving surface moves on the optical axis, there is always a correspondence between the changes in $\triangle F'MN \sim \triangle F'DE$. According to the similarity triangle theorem, it is known that

$$C = \frac{S_{in}}{S_{out}} = \left(\frac{f'}{L}\right)^2 \tag{8}$$

where S_{in} is the input surface area; S_{out} is the output surface area, and h is the distance between the receiving surface and the focus on the optical axis. Therefore, the magnitude of the concentration ratio is related to the position of the receiving surface on the optical axis, and the concentration ratio of the system is larger when the receiving surface is closer to the focal position.

In the design of this paper, the parameters of the Fresnel lens include focal length $f' = 100$ mm, lens radius R = 100 mm, and tooth pitch b = 0.5 mm; the lens material is PMMA, with a refractive index n = 1.49

The radius of the uniform distribution light source is 50 mm, with total of 5962 rays, and the position is 50 mm in front of the Fresnel lens. The solar spectrum is simulated in TracePro. Due to the complexity of the data, we simplified the solar spectrum based on

NASA solar data and considered the irradiance and spectral weight. The resulting spectral data are shown in Table 1.

Table 1. Simulation of solar spectral wavelength.

Wavelength (nm)	Irradiance (W/m^2)	Weight
348	442.887	0.027
415	1171.89	0.028
440	1301.5	0.024
460	1599	0.029
480	1627.7	0.032
500	1548.2	0.033
515	1600.17	0.032
540	1550.2	0.032
560	1617.23	0.032
585	1536.466	0.047
615	1496.178	0.047
645	1466.355	0.048
675	1399.986	0.046
710	1316.3	0.054
755	1197.278	0.059
805	1086.402	0.056
860	978.5	0.062
940	259.192	0.061
1025	767.408	0.057
1135	189.581	0.062
1365	32.517	0.065
1860	2	0.068

According to the above parameters, a three-dimensional model of the Fresnel lens is built in TracePro, and the optical path diagram for tracing the light is shown in Figure 4a.

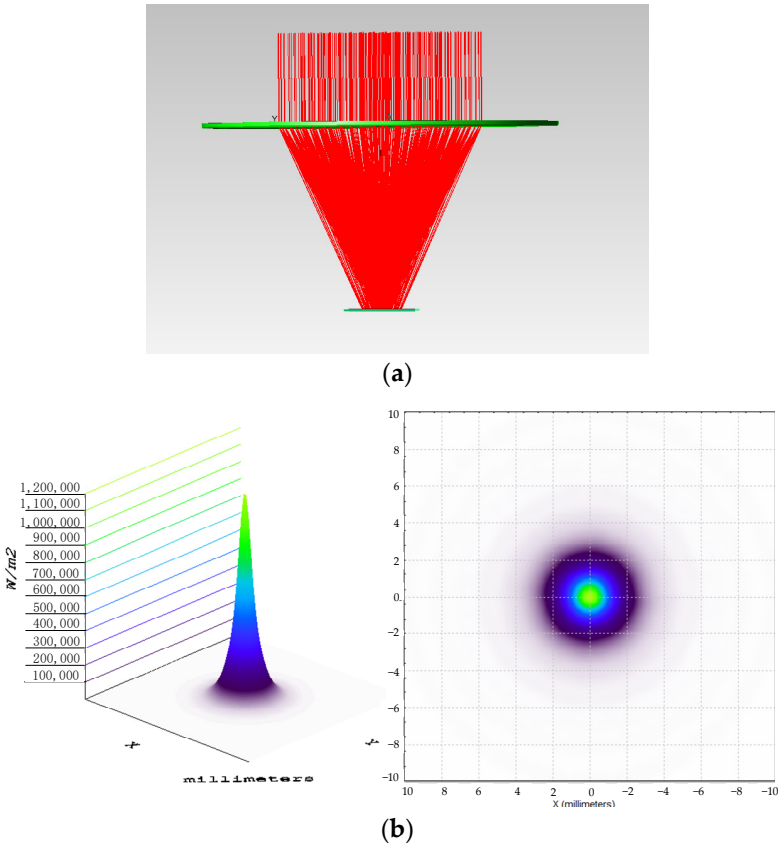

(**a**)

(**b**)

Figure 4. Fresnel lens ray-tracing simulation. (**a**) Optical path when sunlight is incident vertically on a Fresnel lens. (**b**) Fresnel lens spot after concentrating.

As can be seen from Figure 4b, the sun rays converge into a spot 3 mm in radius through the Fresnel lens. The energy is highly concentrated in the spot of a 0.5 mm radius with a maximum value of 1.189×10^6 W/m^2. The concentration ratio is 1089 times, indicating that the designed Fresnel lens has very good concentration performance.

The inhomogeneous light spots produced by the converged light can greatly reduce the photoelectric conversion efficiency of the PV cell and even seriously burn the cell [21]. In order to homogenize the high-energy density light gathered by the Fresnel lens, we installed a quartz concave cavity between the Fresnel lens and the photovoltaic panel. According to the characteristics of the concave lens, it can change the light transmission path [22] to improve the uniformity of the light spot.

2.2. Design of Hollow Concave Cavity Spectral Splitter

The concave cavity consists of a parabolic surface on one side and a flat surface on the other. When the focus of the Fresnel lens coincides with the focus of the hollow concave cavity, the concentrating rays can be refracted by the hollow concave cavity to obtain uniform parallel rays. A geometric structure of the Fresnel lens and hollow concave cavity structure was established, as shown in Figure 5.

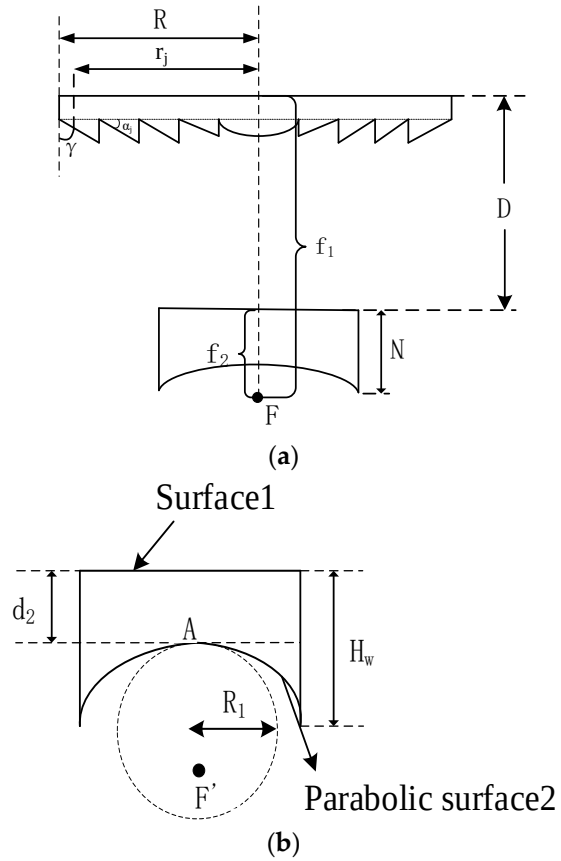

Figure 5. Geometric structure of Fresnel lens and hollow concave cavity. (**a**) System geometry structure. (**b**) Geometric parameters of the concave cavity.

Make the radius of the Fresnel lens R, the focal length f_1, the focal point F, and the inclination angle of each ring band α_j. The radius of curvature of the ring band is r_j. The ring band radius of curvature is r_j. The thickness of the center of the cavity is d_2. H_w is the distance between the receiving surface of the cavity and surface 1. The geometric

parameters are shown in Figure 5. The minimum effective radius of the parabolic surface 2 is set to R_1, and the equation of the parabolic surface 2 in the hollow concave cavity is

$$4f_2z = x^2+y^2,\ f_2 \geq \frac{R_1^2}{4(H_w - d_2)} \tag{9}$$

where f_2 is the focal length of the paraboloid.

According to the principle of geometric optics, light rays passing through the focal point of a concave lens will be emitted parallel to the symmetry axis of the concave lens. Therefore, the focal point F of the paraboloid on the concave cavity must coincide with the focal point F′ of the Fresnel lens:

$$f_1 = f_2 + D \tag{10}$$

Two types of concentrating structures were established in TracePro. The light source is set as a circular lattice point light source, the intensity of the light is 1000 W/m^2, the thickness of the concave H_w is 2 mm, the focal length of the Fresnel lens f_1 is 100 mm, the distance D between the Fresnel lens and concave lens is 70 mm, the focal length of the hollow concave cavity f_2 is 30 mm, and the optical path diagram for ray tracing is shown in Figure 6.

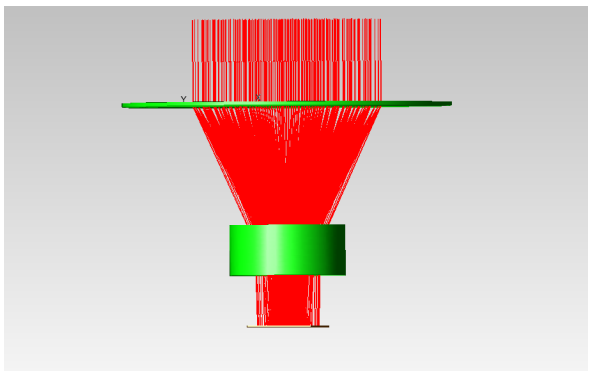

Figure 6. Ray tracing when sunlight is incident on the hollow concave cavity.

ΔE is used to measure the uniformity of solar energy flux density received by the photovoltaic surface. ΔE_{max} indicates the maximum light intensity of the receiving surface; ΔE_{mean} indicates the average light intensity on the receiving surface:

$$\Delta E = 1 - \frac{\Delta E_{max} - \Delta E_{mean}}{\Delta E_{max} + \Delta E_{mean}} \times 100\% \tag{11}$$

A comparative analysis of the spot after receiving the concentrated light on the cell surface is shown in Figure 7.

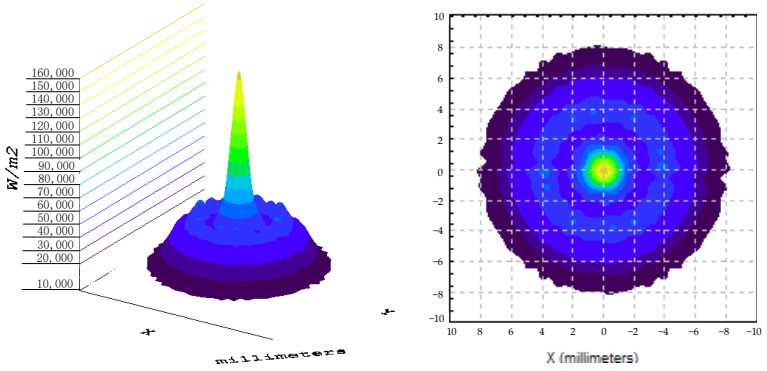

Figure 7. The light spot after concave cavity uniforming.

As seen in Figure 7 and Table 2, after setting up the concave cavity to uniformly distribute the light, the focused spot radius received by the PV cell surface is 8 mm, the peak energy flow density is reduced by 7.6 times, the average energy flow density is 17,806 W/m^2, the spot uniformity is (relatively) improved by 17%, and the optical performance has a great advantage compared to direct light concentration.

Table 2. Optical performance of the splitter using different structures.

Optical Performance	Directly Concentrating	Combined Concentrating
Maximum energy flow density W/m^2	1.189×10^6	1.5629×10^5
Average energy flow density W/m^2	18,815	17,806
Spot uniformity ΔE	4%	21%
Spot radius/mm	3	8

After setting the concave cavity to homogenize the light, the spot is distributed in a series of concentric rings. The maximum energy density is located on the ring with a radius of 1 mm, and a band width of 0.5 mm, and the maximum energy flow density is 1.5629×10^5 W/m^2. The energy flow density of the rest of the ring bands is close to the average value of 17,806 W/m^2. The uniformity of the energy flow density is improved by 17% when compared to direct concentration.

The splitter consists of a concave cavity and a liquid spectral-splitting medium. From the above analysis, it is clear that the concave cavity has a good effect on uniform energy flow. By opening holes on both sides of the concave cavity, the spectral-splitting medium can flow in and out. When the system works, the liquid medium fills the inside of the hollow concave cavity. It is used to split the solar spectrum energy on the one hand and can be used as a heat transfer medium to absorb the infrared light energy from the sunlight on the other hand.

2.3. Performance of the Spectral-Splitting Medium

Common spectral-splitting media include thermal oils or alcohols, and post-configured liquids can also be selected, such as nanofluids [23]. The selected liquid medium should have the following properties:

1. The spectral performance of the liquid medium should match the spectral response band of the PV cell. The light in the cell response band should be transmitted as much as possible and absorbed as much as possible in the nonworking band;
2. Good thermal conductivity, boiling point, stability, and fluidity.

The physical properties of different spectral splitting media are shown in Table 3. ZnO nanofluid has a high spectral transmittance in the range of 400~1100 nm, while the spectral transmittance in the range of 1500~2400 nm is almost zero. It has a large specific heat capacity and good thermal conductivity. Based on the spectral response characteristics of the GaAs cell and the analysis of the physical properties of various spectral-splitting media in the experiment, the ZnO nanofluid was selected as the spectral-splitting medium in this paper.

Table 3. Physical properties of different liquid spectral-splitting media.

Liquid Media	Boiling Point (K)	Transmission Spectrum Wavelength (nm)	Specific Heat Capacity (J·kg^{-1}·K^{-1})	Thermal Conductivity (W·m^{-1}·K^{-1})
Propylene glycol	457	300–1100	2510	0.206
Glycerol	563	300–1000	2350	0.29
5 g/L $CoSO_4$	603	580–1000	4128	0.613
ZnO Nanofluid	973	400–1000	2624	0.218

2.4. Selection of Concentrating PV Cell

In photovoltaic systems, the commonly used types of photovoltaic cells are monocrystalline silicon cells, polycrystalline silicon cells, and concentrator-type silicon cells. Table 4 shows the material characteristics of different types of solar cells [24].

Table 4. Characteristics of different types of solar cell materials.

Types of PV Cell		Band Gap (eV)	Available Spectral Range (nm)	Conversion Efficiency
Silicon PV cell	monocrystalline silicon	1.12	400–900	20%
	polysilicon	1.12	400–950	17%
	Amorphous silicon	1.8	350–750	10.2%
III–V PV cell	GaAs	1.42	400–900	22%
	INP	1.35	1300–1700	24.2%

GaAs cells have obvious advantages: first, this type of cell can operate under light-concentrating conditions. Second, under concentrating conditions, the variation in the cell's electrical parameters due to temperature is relatively small. When the light intensity changes drastically, the temperature of the cell increases significantly, leading to a decrease in efficiency. However, when compared to the increase in sunlight intensity, the decrease in efficiency of the GaAs cell is relatively small. This appearance reflects the significant advantage of GaAs cells over ordinary photovoltaic cells in responding to temperature changes. Therefore, GaAs cells were chosen in this paper.

3. System Model Based on Energy Conservation

On the basis of the mathematical model designed for each subsystem, the energy transfer process is analyzed according to the characteristics of conversion, storage, and transmission of the system. Analytical models of photoelectric and photothermal conversion efficiency were established. The system energy flow model is shown in Figure 8.

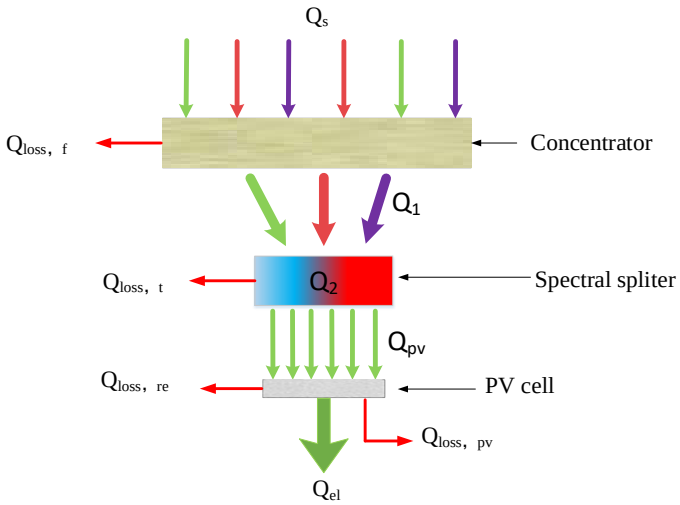

Figure 8. System energy flow model.

The solar radiation Q_s concentrates and irradiates via the spectral splitter through the Fresnel lens, and some solar light is absorbed by the spectral-splitting medium and is converted into thermal energy Q_2. The rest of the solar radiation Q_{pv} is transmitted through the spectral splitter to reach the PV cell. In the process of absorbing heat, a small amount of thermal energy $Q_{loss,t}$ is lost to the environment in the form of radiation. The energy radiated to the surface of the photovoltaic cell is Q_{pv}.

Although the nanofluid absorbs most of the ineffective radiant energy and avoids a significant increase in the temperature of the cell, there are still some bands of solar

radiation that will be converted into thermal energy, which leads to an increase in the temperature of the cell. A small portion of the energy $Q_{loss,re}$ is reflected by the cell's surface, and the remaining energy translates into photovoltaic conversion Q_{el}.

3.1. Energy Analysis of Fresnel Lens Concentrating Module

A Fresnel lens inevitably incurs energy loss during the concentration process. Ke Cao [25] established an energy model of a Fresnel lens to calculate the structural loss and reflection loss of the lens. When the ring band inclination does not exceed the critical angle range, the structural loss can be ignored; then, the reflection loss is the main loss. There are concentric rings on the lens surface. The transmittance of a single ring of the lens is influenced by the refractive index of the lens material and the inclination of the ring, as shown in Equation (12):

$$\Phi = f\ (\delta_n, \theta) \tag{12}$$

where δ is the refractive index of the Fresnel lens material; θ is the inclination angle of the ring band. In the solar spectrum, each wavelength carries a different energy, so the total energy of the sunlight is incident on the j ring band after refraction via the lens:

$$Q_1 = \sum_{j=1}^{N} \left(G\pi(r_j^2 - r_{j-1}^2) \sum_{i=1}^{M} \Phi_{i,j}\omega_i \right) \tag{13}$$

where Φ is lens material transmittance; ω is the weighting factor of the discrete model wavelength of the solar spectrum; G is the light intensity per unit area, and W/m^2; r_j is the radius of curvature of the ring band, m.

The efficiency and energy analysis of the lens is performed in turn, as shown in Equations (14)–(16):

$$\eta_{Fre} = \frac{Q_1}{Q_s} \tag{14}$$

$$Q_s = G \cdot A_{Fre} \tag{15}$$

$$Q_{loss,f} = Q_s(1 - \eta_{Fre}) \tag{16}$$

where Q_s is the energy of the sunlight vertically incident on the system; η_{Fre} is the Fresnel lens concentrating efficiency; A_{Fre} is the Fresnel lens area, m^2; $Q_{loss,f}$ is the Fresnel lens structure concentrating loss energy.

3.2. Energy Analysis of Spectral Splitter

Figure 9 shows the AM1.5 solar spectrum and the spectral response curve of a GaAs cell [26]. Spectral response refers to the magnitude of the photo-generated current generated by the collection of photo-generated charge carriers. According to the photovoltaic cell spectral response, a value greater than 0.5 A/W (when the sun wavelength is determined) is the best spectral response band, so GaAs cells that are only in the wavelength range of 400 to 1000 nm of sunlight can be effective in photoelectric conversion.

In order to investigate the optical properties of the ZnO nanofluid, we used a spectrophotometer to test the spectral transmittance of different particle sizes of the ZnO nanofluid. The test results for the ZnO nanofluid with different particle sizes are shown in Figure 10. It can be seen that the ZnO nanofluid has high spectral transmittance at 400–760 nm. As the nanoparticle size increases, the transmission rate in the visible band decreases. This is due to the poor dispersion of larger nanoparticles, which tend to form large agglomerates and cause absorption across the radiation band.

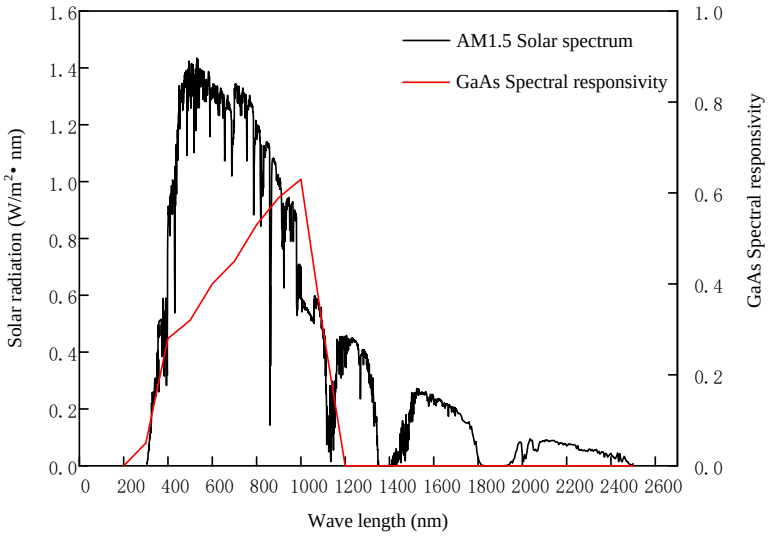

Figure 9. AM1.5 solar spectrum and GaAs cell spectral response.

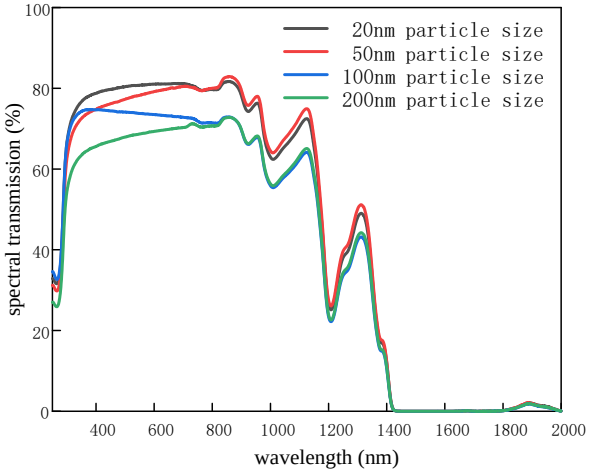

Figure 10. Spectral transmittance of a ZnO nanofluid of different particle sizes.

The spectral G' that reaches the PV cell after the spectral splitting is calculated:

$$G'(\lambda) = G(\lambda) \cdot \tau \tag{17}$$

where $G(\lambda)$ is the AM1.5 solar spectrum, W·m^{-2}·nm^{-1}; τ is the spectral transmittance of the spectral splitting medium; λ is the wavelength, nm.

3.3. Photoelectric Conversion Subsystem

The photovoltaic conversion subsystem is used to convert solar energy into electrical energy after spectral splitting. It is mainly composed of photovoltaic cells, batteries, and DC-AC inverters. The main parameters affecting the photovoltaic conversion characteristics of the system are the area of the photovoltaic cells, the properties of the incident light, and light intensity. The short-circuit current value of a PV cell is linearly related to the concentration ratio when it receives concentrated, high-energy-density sunlight. When combined with the structure of the photovoltaic and spectral splitting concentration solar system, the short-circuit current $I_{sc,c,bs}$ of the PV cell is

$$I_{sc,c,bs} = C \cdot \eta_{fre} \cdot A_{pv} \cdot \int_{280}^{2500} G'(\lambda) \cdot SR(\lambda) d\lambda \tag{18}$$

where $G'(\lambda)$ is the spectral distribution of the PV cell after spectral splitting, and $SR(\lambda)$ is the spectral response characteristic of the GaAs cell.

When the spectral splitting wavelength is within the spectral range of λ_1~λ_2, the open circuit voltage of the solar cell under the irradiance of C times concentration is

$$V_{\mathrm{oc,c,bs}} = \frac{\mathrm{hc}V_{\mathrm{oc}}}{\lambda_2 E_g} + n_f V_{\mathrm{th}} \ln(C) \tag{19}$$

where V_{oc} represents the open-circuit voltage without concentrated light, E_g represents the band gap of the PV cell, h is Planck's constant, c is the speed of light in a vacuum, and n_f denotes the ideal diode factor.

The photothermal potential is defined as

$$V_{\mathrm{th}} = \mathrm{k_B} T_{\mathrm{PV}} / e \tag{20}$$

where e denotes the charge of the electrons, T_{PV} is the temperature of the PV cell, and $\mathrm{k_B}$ is the Boltzmann constant.

The empirical formula for the filling factor FF can be expressed as

$$FF = \frac{v_{\mathrm{oc}} - \ln(v_{\mathrm{oc}} + 0.72)}{v_{\mathrm{oc}} + 1} \tag{21}$$

In the above equation, $v_{\mathrm{oc}} = (V_{\mathrm{oc}}/V_{\mathrm{th}})$, the effect of temperature on voltage is considered in Equation (20). The temperature coefficient [27] is introduced in order to consider the effect of higher temperatures on the efficiency of PV cells under concentrated light conditions, and the photovoltaic conversion efficiency can be calculated using Equation (22):

$$\eta_{\mathrm{pv}} = \frac{FF \cdot V_{\mathrm{oc,c,bs}} \cdot I_{\mathrm{sc,c,bs}}}{C \cdot G_{\mathrm{pv}} \cdot \eta_{\mathrm{fre}} \cdot A_{\mathrm{pv}}} \cdot [1 - E_t \Delta t_{cell}] \tag{22}$$

where E_t is the temperature coefficient of photovoltaic cell, and Δt_{cell} is the variation between the cell temperature and the standard test temperature of the cell (25 °C). The necessary parameters for calculating the conversion efficiency of the PV cell are shown in Table 5.

Table 5. Parameters of the GaAs cell.

Parameter	Value
cell temperature coefficient/E_t	0.0023
V_{oc} (V)	0.965
diode ideal factor/n_f	0.8
cell band gap/E_g	1.45
GaAs density (kg/m^3)	5320
GaAs specific heat capacity (J/(kg·°C))	327

3.4. Photothermal Conversion Subsystem

After the concentration of the sunlight by the concentrator, the nanofluid absorbs solar radiation in a specific wavelength band to heat up. When considering the time term Δt, $Q_2{}^{\mathrm{t}}$ is the final solar radiation received by the nanofluid after concentration and is calculated using Equation (23):

$$Q_2^{\mathrm{t}} = C \cdot G \cdot \eta_{\mathrm{fre}} \cdot \tau_{\mathrm{t}} \cdot A_{\mathrm{fre}} \cdot \Delta t \tag{23}$$

where τ_{t} is the transmittance of the splitter surface.

When the system is in a working state, the nanofluid is injected into the hollow concave cavity until it is full so that the nanofluid inside the container is under concentrated sunlight irradiation. Assuming that the system heat transfer process is always in a steady state, the splitter is made from optical glass with high light transmission and low absorption, and

the absorbing solar radiation via the spectrum splitter is ignored to simplify the calculation. We assume that part of the solar radiation energy absorbed by spectral-splitting medium is converted into internal energy, and the remaining part is converted into heat loss from the outer wall of the splitter:

$$\Delta Q = Q_2^t\left(1 - \tau_{fluid}\right) - Q_{loss,t} = c_{flu} m_{flu} \frac{\partial T_b}{\partial t} \tag{24}$$

where ΔQ is the variation in internal energy of the nanofluid in the splitter, J; c_{flu} is the specific heat capacity of the nanofluid, J/(kg·°C); m_{flu} is the mass flow rate of the nanofluid in the splitter, kg/s; T_b is the fluid temperature at an arbitrary moment, °C. According to the energy balance Equation (24), the final temperature of the nanofluid can then be calculated.

τ_{fluid} denotes the average transmittance of the nanofluid, which can be expressed by Equation (25):

$$\tau_{fluid} = \int_{280}^{2500} G(\lambda)\tau(\lambda)d\lambda / \int_{280}^{2500} G(\lambda)d\lambda \tag{25}$$

For the heat dissipation process of the splitter, it mainly includes radiation heat dissipation loss and convective heat dissipation loss:

$$Q_{loss,t} = A_t \cdot \varepsilon_t \cdot \sigma \cdot \left(T_b^4 - T_{amb}^4\right) + A_t \cdot h_t \cdot (T_b - T_{amb}) \tag{26}$$

where A_t is the heat collection area of the splitter; ε is the emissivity of the splitter; σ is the Stephan-Boltzmann constant; T_{amb} is the ambient temperature. h_t is the heat transfer coefficient of convection between the splitter and air. This parameter is a function of wind speed v [28] and can be calculated using Equation (27):

$$h_t = 2.8 + 3v \tag{27}$$

As the temperature of the PV cell is higher than the ambient temperature, part of the radiant energy is converted into thermal energy $Q_{loss,pv}$, which dissipates into the environment. Therefore, the direction of heat transfer is from the surface of the PV cell to the surrounding environment. Assuming that the surface absorption rate of the cell module is Δ_{pv}, the energy balance equation of the PV cell can be expressed as

$$Q_2^t - Q_2^t \cdot (1 - \partial_{pv}) - Q_{loss,pv} - Q_2^t \cdot \eta_{pv} = L_{pv} \cdot A_{pv} \cdot \rho_{pv} \cdot C_{pv} \cdot \frac{\partial T_{pv}}{\partial t} \tag{28}$$

where ∂_{pv}, L_{pv}, C_{pv}, ρ_{pv}, and T_{pv} are the absorption rate, thickness, specific heat capacity, density, and temperature of the GaAs cell, respectively.

Therefore, the temperature of the PV cell can be determined by using Equation (28).

$$Q_{loss,pv} = A_{pv} \cdot \varepsilon_{pv} \cdot \sigma \cdot \left(T_{pv,1}^4 - T_{amb}^4\right) \tag{29}$$

The thermal efficiency of the subsystem is calculated using Equation (30).

$$\eta_{th} = \frac{c_{flu} \cdot m_{flu} \cdot (T_b' - T_b)}{C \cdot G \cdot \eta_{fre} \cdot A_t} \tag{30}$$

3.5. System Overall Electrical Efficiency

After absorbing heat and raising the temperature, the nanofluid is assumed to be a high-temperature heat source. The collected solar radiation energy is used in a heat engine to generate electricity. For this form of power generation, the overall electrical efficiency of

the comprehensive solar energy utilization system based on photovoltaic concentration and spectral splitting can be expressed as

$$\eta_{\mathrm{sys}} = \eta_{\mathrm{pv}} + \eta_{\mathrm{th}} \cdot K \cdot \left(1 - \frac{T_{\mathrm{amb}}}{T_{\mathrm{b}}}\right) \tag{31}$$

where T_0 denotes the ambient temperature, and $(1 - T_{\mathrm{amb}}/T_{\mathrm{b}})$ denotes Carnot cycle efficiency.

$$K = \frac{\varepsilon \cdot \eta_{\mathrm{pv}} + \eta_{\mathrm{th}}}{\varepsilon \cdot \eta_{\mathrm{pv,0}}} \tag{32}$$

ε denotes the photothermal conversion ratio of a typical thermal power plant, which usually converts three units of thermal energy into one unit of electrical energy [29], so ε is taken as 3 in this paper. $\eta_{\mathrm{pv,0}}$ denotes the photoelectric conversion efficiency of the system when the light is not concentrated and spectral split.

4. Efficiency Analysis of Comprehensive Solar Utilization System

By analyzing the energy flow model for the above system, it can be seen that the model of the comprehensive solar utilization system mainly includes the energy balance equations of the Fresnel lens, hollow concave cavity, spectrum-splitting nanofluid, GaAs cell, and other components.

4.1. Model Establishment and Solution

The mathematical model of the system was established by synthesizing Equations (13)–(32), and the system was simulated using Matlab. When calculating the temperature of the photovoltaic cell nanofluid, we set the calculation accuracy of the photovoltaic cell and nanofluid to 1 °C as the convergence principle. Based on the above steps, the system model calculation process is shown in Figure 11.

All calculation results are based on a spectral-splitter receiving area of 0.1 m^2, with an initial time t = 0 s and a time step size Δt = 60 s. According to the mathematical model of the system, the efficiency model is used to analyze the effects of solar irradiance and the concentration ratio on the characteristics of the system. The ambient temperature T_{b} is 25 °C. The initial temperature T_{pv} of spectral-splitting fluid is 25 °C, with the system design parameters shown in Table 6.

Table 6. Design parameters of the system.

Parameter	Value
Refractive index of Fresnel lens σ_{n}	1.49
Transmittance of Fresnel lens τ	0.95
Concentrating efficiency of Fresnel lens η_{Fre}	0.75
Hollow concave cavity area $A_{\mathrm{t}}/\mathrm{cm}^2$	10
Liquid spectral splitting medium mass flow rate kg/s	1×10^{-3}
Emissivity of hollow concave cavity ε_{c}	0.9
Surface transmittance of hollow concave cavity τ_{t}	0.9
Average transmittance of ZnO nanofluids τ_{fluid}	0.3
Specific heat capacity of ZnO nanofluids J/(kg °C)	2.624×10^3
Emissivity of GaAs $\varepsilon_{\mathrm{pv}}$	0.9
GaAs area $A_{\mathrm{pv}}/\mathrm{cm}^2$	10
GaAs cell thickness L_{pv}/cm	2×10^{-3}
Environmental wind speed $v/\mathrm{m{\cdot}s^{-1}}$	0.5

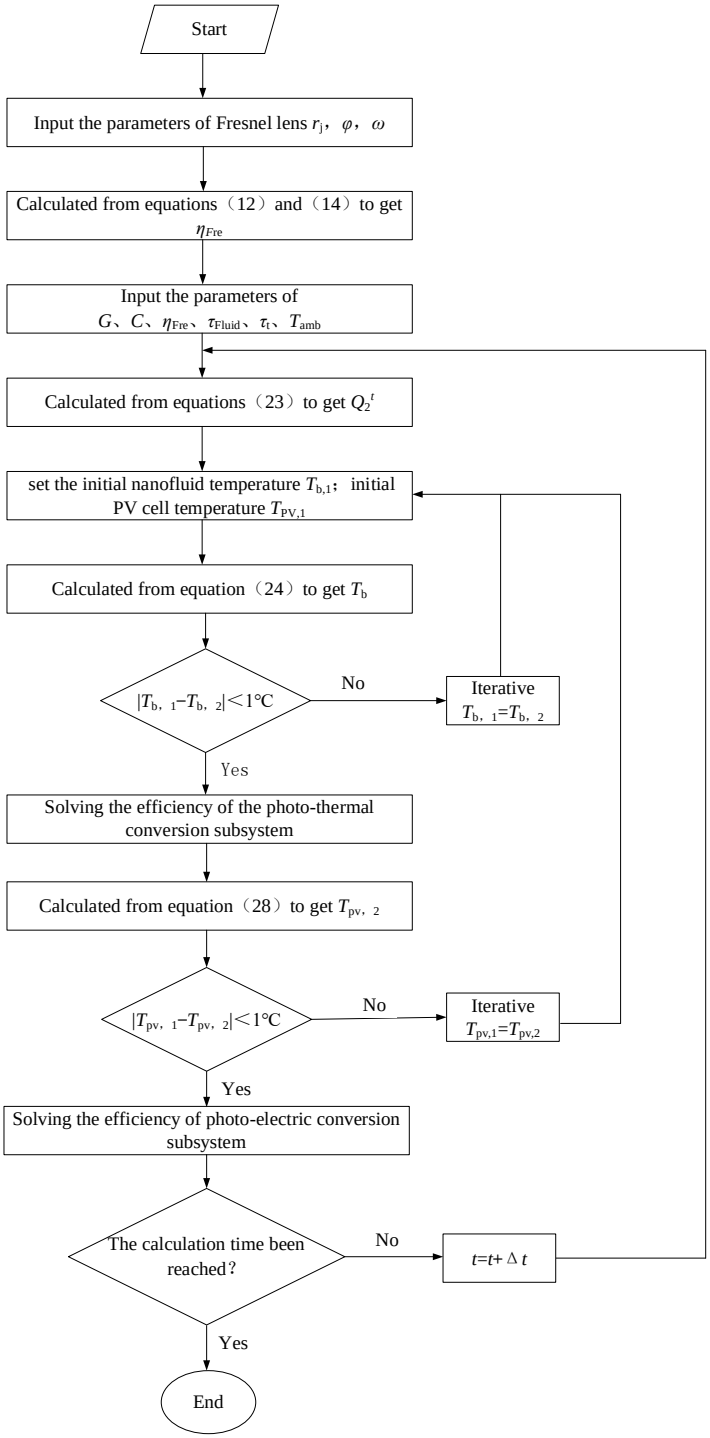

Figure 11. System efficiency program calculation process.

4.2. Analysis of Solar Irradiance on the Photoelectric and Photothermal Efficiency of the System

According to the basic parameters of the solar utilization system based on photovoltaic concentration and spectral splitting, shown in Table 6, the influence of photothermal efficiency by solar irradiance was analyzed under the condition of a concentration ratio 50 times that of concentrated light. The results are shown in Figure 12.

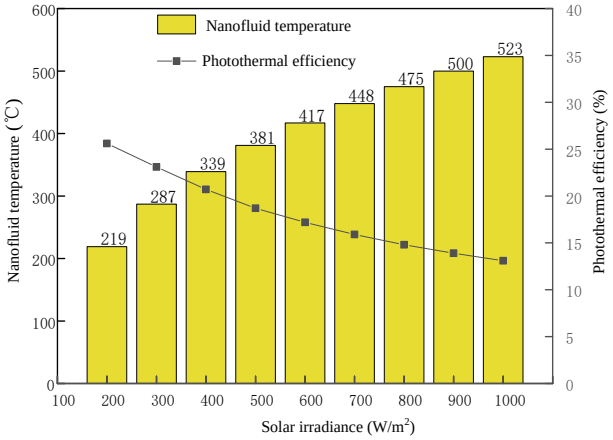

Figure 12. Effect of solar irradiance on photothermal efficiency and nanofluid temperature.

It can be seen that the maximum conversion efficiency of the photothermal conversion subsystem is 25.6%. With an increase in solar radiation, the efficiency of the photothermal conversion decreases gradually. This is because the heat dissipated into the air by the nanofluid gradually increases with the rise in nanofluid temperature, which makes the photothermal conversion efficiency decrease. The nanofluid temperature gradually rises with the increase in solar irradiance, reaching a maximum of 523 °C at 1000 W/m^2.

Figure 13 shows that when the concentration ratio is 50 times, the temperature of the GaAs cells will increase with enhanced solar irradiance. When solar irradiance is 1000 W/m^2, the temperature of the cells rises to 607 °C, which greatly affects conversion efficiency and even burns the cell. The nanofluid in the splitter absorbs most of the infrared light energy from solar radiation, making the temperature of the cell only slightly increase with solar irradiance. When solar irradiance is 1000 W/m^2, the temperature of the cell is 106 °C, and it can still work normally. It can be seen from the comparison that under concentrated light, the splitter can significantly reduce the temperature of the cell.

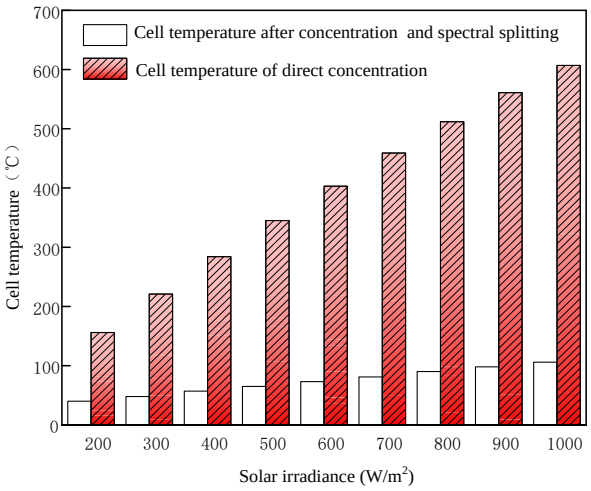

Figure 13. Cell temperature at different solar irradiances.

As can be seen in Figure 14, the photovoltaic cells are affected by temperature coefficients, and the efficiency without spectral-splitting cells will be greatly reduced. When spectral splitting to make the temperature of the concentrated photovoltaic cells greatly reduced, the photoelectric conversion efficiency is at least 7% higher than the efficiency of nonspectral-splitting cells. When solar irradiance is greater than 600 W/m^2, the photoelectric conversion efficiency of the photovoltaic cell without spectral splitting is almost reduced to 0 due to the high temperature, while the photoelectric conversion efficiency

of the cells only decreases by 4.35% after spectral splitting. The photovoltaic efficiency of direct concentration systems decreases significantly when solar irradiance increases. Through spectral splitting, it is possible to obtain higher photovoltaic efficiency while increasing the concentration ratio of the system.

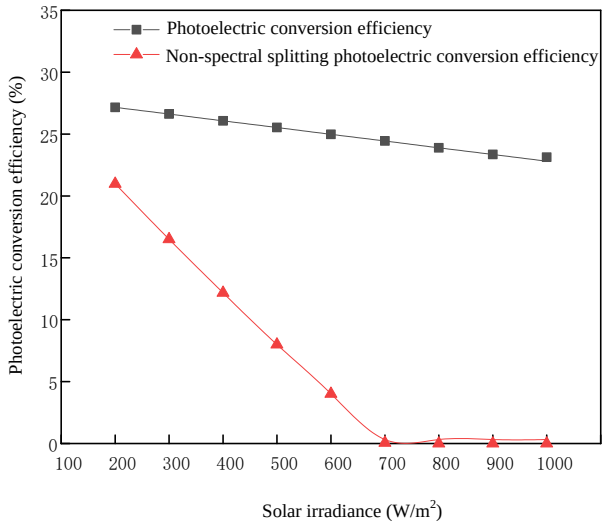

Figure 14. Photoelectric conversion efficiency of different solar irradiances.

4.3. Analysis of the Concentration Ratio on the Electric-Thermal Characteristics

Figure 15 shows that with an increase in concentration ratio, the photoelectric conversion and the photothermal conversion efficiency of the system will decrease. The reason for this is that when the Fresnel lens with a higher concentration ratio is used, the amount of thermal radiation to the PV cell will also increase, which will lead to a decrease in photoelectric conversion efficiency. At the same time, more solar radiation will be absorbed by the nanofluid and will be converted into thermal energy. As the temperature of the nanofluid increases, the heat loss of the nanofluid increases, leading to a decrease in the average thermal efficiency of the system, which, in turn, leads to a corresponding decrease in the overall efficiency. However, the value of the concentration ratio still needs to be considered in conjunction with the actual required thermal fluid temperature (not the lower, the better).

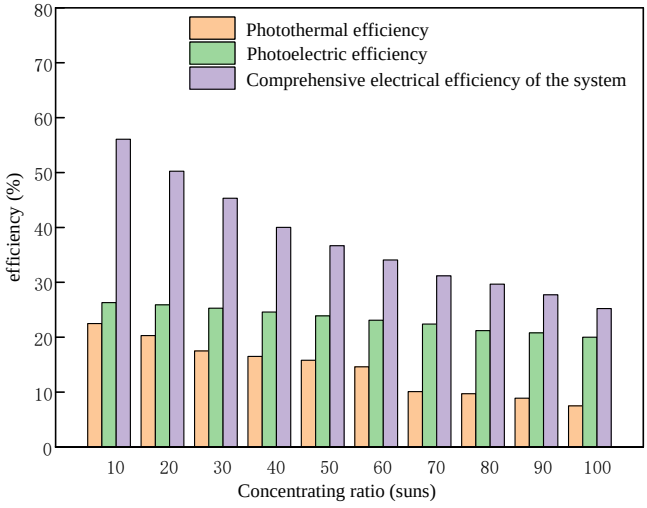

Figure 15. System efficiency with different concentration ratios.

5. Conclusions

This paper proposes a new solar energy comprehensive utilization system based on a Fresnel lens concentrator and spectral splitting. A geometric model of Fresnel lenses and a hollow concave cavity was established to analyze the optical performance of the system by using the Monte Carlo ray-tracing method. Meanwhile, an energy model of photoelectric and photothermal conversion was built based on the process of energy transfer in the system. The effects of solar irradiance and concentration ratio on system performance were analyzed. The following conclusions were obtained:

1. By installing a quartz concave cavity between the Fresnel lens and PV cell, the uniformity of the spot irradiated is improved. The maximum energy flux density is 1.5629×10^5 W/m^2, and the average value is 17,806 W/m^2. The uniformity of the focused spot has been improved by 17% when compared to direct focusing;
2. By opening holes on both sides of the hollow concave cavity, the ZnO nanofluid can flow in from one side and out from the other side. During the photothermal conversion process, the ZnO nanofluid can split the solar spectral energy. On the other hand, it can be used as a heat transfer medium to absorb the infrared light energy from sunlight as a heat source;
3. After numerical simulation, the results show that, when compared to nonspectral splitting, there is only a small increase in the temperature of the PV cell with spectral splitting. At a concentration ratio of 50 and a light intensity of 1000 W/m^2, the cell temperature increases by 81 °C, and the photoelectric conversion efficiency increases by 0.81%. When compared to direct concentration, the photoelectric conversion efficiency is increased by at least 7%. Meanwhile, when solar irradiance is 1000 W/m^2, a nanofluid with a temperature of 523 °C can be obtained, with a comprehensive electrical efficiency of 36.7%.

Author Contributions: Conceptualization, Z.H. and Y.T.; Methodology, Z.H.; Software, Z.H.; Validation, Z.H. and Y.T.; Formal Analysis, Z.H.; Investigation, Z.H.; Resources, Z.H.; Data Curation, Z.H.; Writing—Original Draft Preparation, Z.H.; Writing—Review & Editing, Y.T.; Visualization, Y.T.; Supervision, Y.T.; Project Administration, Y.T.; Funding Acquisition, Y.T. All authors have read and agreed to the published version of the manuscript.

Funding: Sponsored by the Natural Science Foundation of Xinjiang Uygur Autonomous Region (2022D01C364).

Data Availability Statement: The data that supports the findings of this study are available within the article.

Conflicts of Interest: The authors declare no conflict of interest.

References

1. Kumari, S.; Bhende, A.; Pandit, A.; Rayalu, S. Efficiency enhancement of photovoltaic panel by heat harvesting techniques. *Energy Sustain. Dev.* **2023**, *73*, 303–314. [CrossRef]
2. Hao, G.Q.; Yuan, A.Y.; Li, H.B. Concentrating photovoltaic technology research. *Chin. J. Power Sources* **2017**, *41*, 1217–1220.
3. Li, L.L.; Bai, Y.; Huang, H.Y. Progress in research and application of hybrid solarphotovoltaic/thermal collectors. *Chin. J. Power Sources* **2017**, *41*, 1217–1220.
4. Wu, X.L.; Shu, B.F.; Lian, R.H.; Wang, J. The performance of v-shaped trough low-power concentrated photovoltaic solar thermal integra-tion components. *Sci. Technol. Eng.* **2018**, *18*, 191–199.
5. Xu, X.P.; Jiang, S.N. Research Status of Concentrate Photovoltaic Power Generation System and Design Requirements of Concentrate module. *J. Chang. Univ. Sci. Technol.* **2019**, *42*, 1–6.
6. Bai, H.L.; Wang, C.; Lu, J. Solar cell heat dissipation technology and development status of concentrating photovoltaic system. *Chem. Ind. Eng. Prog.* **2023**, *42*, 159–177.
7. Jin, Z.L.; Ji, J.; Xu, N.; Li, J. Experiment study of a point-focus fresenel high concentrator photovoltaic/thermal system. *Acta Energ. Sol. Sin.* **2018**, *39*, 69–75.
8. Ju, X.; Vossier, A.; Wang, Z.F.; Dollet, A.; Flamant, G. An improved temperature estimation method for solar cells operating at high concentrations. *Sol. Energy* **2013**, *93*, 80–89. [CrossRef]

9. Mojiri, A.; Taylor, R.; Thomsen, E.; Rosengarten, G. Spectral beam splitting for efficient conversion of solar energy—A review. *Renew. Sustain. Energy Rev.* **2013**, *28*, 654–663. [CrossRef]
10. Zhang, J.J.; Qu, Z.G.; Wang, Q.; Zhang, J.F.; He, Y.L. Multiscale investigation of the plasmonic solar cell in the spectral splitting concentrating photovoltaic-thermal system. *Energy Convers. Manag.* **2021**, *250*, 114846. [CrossRef]
11. Wang, G.; Yao, Y.B.; Lin, J.Q.; Chen, Z.S.; Hu, P. Design and thermodynamic analysis of a novel solar CPV and thermal combined system utilizing spectral beam splitter. *Renew. Energy* **2020**, *155*, 1091–1102. [CrossRef]
12. Crisostomo, F.; Robert, A.; Zhang, T. Experimental testing of SiNx/SiO_2 thin film filters for a concentrating solar hybrid PV/T collector. *Energy Ecol. Bus.* **2014**, *72*, 79–87.
13. Zhang, G.M.; Wei, J.J.; Xie, H.L.; Wang, Z.X.; Xi, Y. Muhammad Khalid. Performance investigation on a novel spectral splitting concentrating photovoltaic/thermal system based on direct absorption collection. *Sol. Energy* **2018**, *163*, 552–563. [CrossRef]
14. Han, X.Y.; Xue, D.S.; Guo, Y.J.; Qu, J. Optical properties analysis of liquid based selective beam-splitting filter for concentrating PV/T beam splitting applications. *J. Eng. Thermophys.* **2017**, *38*, 2313–2319.
15. Chen, X.B.; Han, X.Y.; Sun, Y. Study on propylene glycol based Ag/$CoSO_4$ nanofluid splitter for spectrum-splitting PV/T system. *Acta Energ. Sol. Sin.* **2021**, *42*, 168–173.
16. An, W.; Wu, J.R.; Zhu, T.; Zhu, Q.Z. Experimental investigation of a concentrating PV/T collector with Cu_9S_5 nanofluid spectral splitting filter. *Appl. Energy* **2016**, *184*, 197–206. [CrossRef]
17. Verma, S.; Tiwari, A.K.; Tripathi, M. An evaluative observation on impact of optical properties of nanofluids in performance of photo-thermal concentrating systems. *Sol. Energy* **2018**, *176*, 709–724. [CrossRef]
18. Liang, H.X.; Wang, F.Q.; Zhang, D.; Cheng, Z.M.; Zhang, C.X. Experimental investigation of cost-effective ZnO nanofluid based spectral splitting CPV/T system. *Energy* **2020**, *194*, 116913.
19. Ju, X.; Xu, C.; Han, X.; Du, X.Z.; Wei, G.S.; Yang, Y.P. A review of the concentrated photovoltaic/thermal (CPVT) hybrid solar systems based on the spectral beam splitting technology. *Appl. Energy* **2017**, *187*, 534–563. [CrossRef]
20. Wu, J.R.; Tang, Z.W.; Zhou, Y.Z.; Wang, H. Photothermal properties of point focused transmissive fresnel collector. *Chem. Ind. Eng. Prog.* **2020**, *39*, 55–63.
21. Hu, J.P.; Li, Q. Theoretocal research of uniformity of light spot influence on performance of concentrating silicon cells. *Acta Energ. Sol. Sin.* **2021**, *42*, 23–28.
22. Yan, J.; Nie, D.Z.; Tian, Y.; Liu, Y.X. Optimal design of concave lens for flux homogenization of solar dish/cavity collector system. *Acta Energ. Sol. Sin.* **2021**, *41*, 161–172.
23. Huang, G.; Curt, S.R.; Wang, K.; Markides, C. Challenges and opportunities for nanomaterials in spectral splitting for high-performance hybrid solar photovoltaic-thermal applications:A review. *Nano Mater. Sci.* **2020**, *2*, 183–203. [CrossRef]
24. Zhang, W.W.; Qi, H.; Ji, Y.K.; He, M.J.; Ren, Y.T.; Li, Y. Boosting photoelectric performance of thin film GaAs solar cell based on multi-objective optimization for solar energy utilization. *Sol. Energy* **2021**, *230*, 1122–1132. [CrossRef]
25. Cao, K.; Yuan, D.Z.; Hu, H.M.; Jiang, Y.Y. Study on thermoelectric performance of high-power concentration photovoltaic and thermal integrated system. *Acta Energ. Sol. Sin.* **2021**, *42*, 64–70.
26. Looser, R.; Vivar, M.; Everett, V. Spectral characterisation and long-term performance analysis of various commercial Heat Transfer Fluids (HTF) as Direct-Absorption Filters for CPV-T beam-splitting applications. *Appl. Energy* **2014**, *113*, 1496–1511. [CrossRef]
27. Helmers, H.; Andreas, B.; Parisi, J.; Agert, C. Modeling of concentrating photovoltaic and thermal systems. *Prog. Photovolt. Res. Appl.* **2014**, *22*, 427–439. [CrossRef]
28. An, W.; Li, J.; Ni, J.; Taylor, R.; Zhu, T. analysis of a temperature dependent optical window for nanofluid-based spectral splitting in PV/T power generation applications. *Energy Convers. Manag.* **2017**, *151*, 23–31. [CrossRef]
29. Widyolar, B.; Jiang, L.; Winston, R. Spectral beam splitting in hybrid PV/T parabolic trough systems for power generation. *Appl. Energy* **2018**, *209*, 236–250. [CrossRef]